Asymptotic solutions for turbulent mass transfer at high Schmidt number

Maarten van Reeuwijk[1] & Kaveh Sookhak Lari[2]

[1] *Department of Civil and Environmental Engineering, Imperial College London London SW7 2AZ, United Kingdom*
[2] *Department of Civil Engineering, University of Isfahan, Isfahan 81744-873441, Iran*

We present closed-form solutions for high Schmidt number mass transfer in a hydrodynamically fully developed turbulent flow. Governing equations for the near- and far-field are developed for a large class of boundary conditions (BCs) for which the mass flux is a function of the concentration at the wall. We show that for this class of BCs, which includes nonlinear wall reactions, the mass transfer coefficient is independent of the BC and the Sherwood correlation is therefore universal. For Dirichlet, Neumann and Robin BCs, the far-field solutions are in good correspondence with the method of separating variables and near-field solutions are in good agreement with numerical simulations. However, in contrast with the far-field solutions, the Sherwood correlation in the near-field depends on the specific BC. As an example of nonlinear BCs, solutions for a second order wall reaction are derived which are compared with numerical simulations and found to be in excellent agreement.

Key words: Turbulence, High Schmidt number, Asymptotic solution, Nonlinear Boundary Conditions.

1. Introduction

The exchange of mass and/or heat of a turbulent flow with its bounding surface occurs in several areas of engineering. One classical example is the corrosion of pipe walls due to the presence of a corrosive species in water, such as carbon dioxide (Sydberger & Lotz, 1982; Sarin *et al.*, 2004) or chlorine (Al-Jasser, 2007; Clark & Haught, 2005; Rossman *et al.*, 1994). Another classical example is the heat transfer through conduit walls, as is relevant for e.g. heat exchangers (Bergmann & Fiebig, 1999) and district heating (Webb & Kim, 2005). In this paper, we will concentrate on turbulent mass transfer problems, although the results are equally applicable to heat transport problems where buoyancy effects are negligible.

A typical quantity of interest is the realised mass (heat) flux at the wall, represented by the mass (heat) transfer coefficient and in dimensionless form by the Sherwood number Sh (Nusselt number). They will depend on the Reynolds number Re and the Schmidt number Sc (Prandtl number), the former representing the ratio between inertial and viscous forces, and the latter the ratio between kinematic viscosity and molecular (thermal) diffusivity. These relations often are presented as powerlaws $Sh = b_1 Re^{b_2} Sc^{b_3}$, where b_1, b_2 and b_3 are coefficients.

Determination of these coefficients has been the objective of many experimental, numerical and theoretical investigations and a selection of Sh correlations for high Sc is presented in the supplementary material. The powerlaw exponents depend critically on the near-wall behaviour of the eddy diffusivity and several theoretical models based on theory of turbulent boundary layers have been developed over the years (e.g. Kader & Yaglom, 1972; Aravinth, 2000).

The mass transport equation (see §3) is a linear partial differential equation with variable coefficients. Many analytical methods therefore make use of the method of separating variables (see e.g. Sleicher *et al.*, 1970; Notter & Sleicher, 1971, 1972; Biswas *et al.*, 1993; Weigand *et al.*, 2001; Weigand, 2004), and with great success: the classical power law relationship $Sh = 0.016 Re^{0.88} Sc^{0.33}$ proposed by Notter & Sleicher (1972) remains widely used today (e.g. Rossman *et al.*, 1994). However, there are some drawbacks and limitations to this method. First, the determination of each of the eigenfunctions and eigenvalues has to be done numerically because of the variable coefficients in the problem. Second, the method of separating variables is applicable to linear boundary conditions (BCs) only; obtaining solutions for nonlinear BCs, as of importance for e.g. biofilm growth (Munavalli & Mohan Kumar, 2004; Noguera & Morgenorth, 2004) is generally not possible.

In this paper, we will focus on the development of asymptotic solutions for turbulent mass transport at high Sc and Re for linear (notably Dirichlet, Neumann and Robin) and nonlinear BCs. Closed-form solutions for the near- and far-field will be presented, where the near-field is the region where the concentration boundary layer is developing and the mass transfer coefficient will be dependent on the streamwise direction. The far-field is defined as the region where the mass transfer coefficient has become constant.

There is a long history of asymptotic solutions for developing concentration boundary layers. Analytical solutions for a thermal boundary layer in a fully developed turbulent flow were developed by Linton & Sherwood (1950). The derivation involved neglecting the streamwise advective, diffusive transport and all turbulent transport, thereby essentially reducing the problem to that solved by Lévêque (1928) in the context of heat transfer in a laminar boundary layer. By assuming self-similarity, closed-form solutions for the boundary layer growth and concentration profile and heat transfer could be provided. Electrochemical experiments of high Sc and Re mass transfer in the entrance region (Shaw *et al.*, 1963; Berger & Hau, 1977) showed good agreement between the predictions from the asymptotic solutions and the measurements. Kestin & Persen (1962) developed asymptotic solutions for the heat transfer across a developing boundary layer over a flat plate, including viscous entrance effects. Several solutions were presented, including a transition from a laminar to a turbulent boundary layer and stepchanges in the wall temperature.

Far-field asymptotic solutions for high Sc solutes, however, seem to have escaped attention until recently. Garcia-Ybarra & Pinelli (2006) used matched asymptotic expansions to derive a closed-form solution for the concentration profile for a fixed concentration (Dirichlet) BC at high Sc. Sookhak Lari *et al.* (2010) independently arrived at the same closed-form solution by observing that the scalar flux was approximately constant across the concentration boundary

layer in a study on the decay of residual chlorine in pipes as a result of a first-order reaction with the wall (Robin BC). Despite the different BCs, both studies report the same Sh correlation.

The aim of this paper is to generalise the work of Garcia-Ybarra & Pinelli (2006); Sookhak Lari *et al.* (2010) to much more general BCs and to provide simple closed-form solutions for the mass-transfer, decay coefficients and concentration profiles. After a discussion on the appropriate velocity and turbulent diffusivity profiles (§2), the governing equations for the far-field are derived (§3). It will become apparent that the Sh correlation reported in Garcia-Ybarra & Pinelli (2006); Sookhak Lari *et al.* (2010) is in fact representative for a very large class of BCs (§4). Closed-form solutions for Dirichlet, Neumann and Robin BCs are presented in §5a. We then use the Von Karman-Pohlhausen method to pose the governing equation for the near-field and present solutions in §6. As the solution method is not limited to linear BCs, closed-form solutions for a second order wall reaction are presented (§5b, §6). Concluding remarks are made in §7.

2. Near-wall profiles of velocity and eddy diffusivity

Consider a fully developed turbulent flow field. When $Sc \gg 1$, as is the case for many mass transfer problems (and heat transfer in e.g. heavy oils), the scalar diffuses much slower than momentum. The associated layer of thickness δ_m near the wall where molecular diffusion dominates over turbulent transport, hereafter referred to as the mass transfer boundary layer (MTBL) will then be entirely nested in the viscous wall region (viscous + buffer layer) (Schlichting & Gersten, 2000; Pope, 2000; Garcia-Ybarra & Pinelli, 2006; Sookhak Lari *et al.*, 2010). Outside the MTBL, the turbulence causes sufficient mixing to assume a uniform concentration. The two fundamental parameters governing the viscous wall region are the kinematic viscosity ν and the friction velocity $u_\tau = \sqrt{\tau_w/\rho}$, where τ_w is the wall shear stress, and ρ is the fluid density. In the viscous sublayer, the turbulent stress is negligible, and therefore the average velocity profile is given by (Bird *et al.*, 2002; Pope, 2000; Schlichting & Gersten, 2000)

$$u^+ = y^+ \tag{2.1}$$

where $u^+ = u/u_\tau$ and $y^+ = y/\delta_v$, y represents the distance from the wall and $\delta_v = \nu/u_\tau$ is the viscous lengthscale.

A second property of the viscous sublayer is that the turbulent momentum flux $\overline{v'u'}$, and therefore the eddy-viscosity ν_T, has a cubic dependence on the wall distance

$$\frac{\nu_T}{\nu} = b{y^+}^3 + O({y^+}^4) \tag{2.2}$$

which can be shown using Taylor expansions (Bird *et al.*, 2002; Antonia & Kim, 1991). The prefactor b has been approximated experimentally and numerically, and takes the value $b \approx 9.5 \times 10^{-4}$ (Bird *et al.*, 2002). Using (2.2), the ratio of the turbulence diffusion coefficient D_T to the molecular diffusion coefficient D is given by

$$\frac{D_T}{D} = b\frac{Sc}{Sc_T}y^{+3} + O(y^{+4}) \tag{2.3}$$

where $Sc = \nu/D$ is the Schmidt number and $Sc_T = \nu_T/D_T$ the turbulence Schmidt number. The effective exponent for D_T is crucial for high Sc mass transfer as it influences the Sh correlation: $D_T \sim y^m$ implies that $Sh \sim Sc^{1/m}$. Many laboratory experiments (Harriott & Hamilton, 1965; Mizushina *et al.*, 1971; Dawson & Trass, 1972; Berger & Hau, 1977; Zhao & Trass, 1997) find that $Sh \sim Sc^{0.32-0.35}$, thereby indirectly confirming (2.3). Shaw & Hanratty (1977) report a slightly lower Sc dependence $Sh \sim Sc^{0.29}$, although it is not entirely clear what the cause is for the deviations between this and the other experiments. More information about Sh correlations for high Sc mass transfer, including the range of Sc and Re considered, can be found in the supplementary material.

A Taylor expansion confirms that the turbulent scalar flux is indeed expected to vary as the cubic on wall distance for fixed concentration (Dirichlet) BCs (Bird *et al.*, 2002; Antonia & Kim, 1991; Garcia-Ybarra & Pinelli, 2006). However, for flux (Neumann) BCs, a second order dependence of the turbulent scalar flux (and therefore D_T) on the wall distance is obtained. As the D_T profile at high Sc has not been reported as yet for flux BCs, it is not known how dominant the second order term is. The only available data is from simulations for the heat transfer across a fluid layer and a solid wall with finite thermal conductivity (Tiselj *et al.*, 2004; Bergant & Tiselj, 2007). The simulations show that Sc_T decreases very close to the wall, as expected for a quadratic D_T profile. However, Bergant & Tiselj (2007) report that the influence on the mean temperature profiles and the heat transfer coefficients is almost negligible.

For Dirichlet BCs, studies performed with Direct Numerical Simulation (DNS), show that Sc_T is indeed constant when Sc is of order unity (Antonia & Kim, 1991; Kawamura *et al.*, 1998; Schwertfirm & Manhart, 2007). At $Sc > 10$, an increase of Sc_T is observed very close to the wall ($y^+ < 1$), which becomes more pronounced for higher Sc (Na & Hanratty, 2000; Crimaldi *et al.*, 2006; Schwertfirm & Manhart, 2007; Bergant & Tiselj, 2007; Kozuka *et al.*, 2009). Garcia-Ybarra (2009) used DNS and LES data to show evidence that the fourth order term overwhelms the cubic term a bit further away from the wall, which suggests that the effective exponent for D_T is larger than three. This is consistent with the experiments of Shaw & Hanratty (1977) but not with the other studies mentioned above. Further laboratory experiments and/or Direct Numerical Simulation at higher Re_τ and Sc will be required to settle this issue.

In what follows we will use the classical assumption (e.g. Kader, 1981; Bird *et al.*, 2002) that D_T is a cubic and that Sc_T is constant. Even though this excludes some of the phenomena described above, the net effect of $y-$ variation of Sc_T (the modification of the mass transfer coefficient etc.) can be incorporated by tuning of the parameter b/Sc_T which is discussed in appendix 1. The procedure maps the actual profile for D_T onto a cubic which has the same boundary layer thickness δ_m (defined below), thereby ensuring that integral quantities be predicted accurately. Note that if the profile for D_T differs significantly from a cubic, the parameter b/Sc_T will become dependent on Sc and Re, the consequences of which will be described in §7.

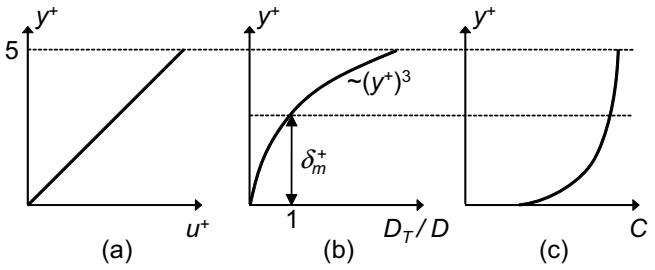

Figure 1. Sketch of the viscous sub-layer and MTBL for high Re and Sc; a) velocity profile; b) eddy diffusivity profile; c) concentration profile.

The properties of the viscous sublayer and MTBL for a high Sc solute are depicted in Fig. 1. Figs 1(a) and 1(b) show the dependence of u^+ and D_T/D on the wall distance, and Fig. 1(c) shows a typical concentration profile valid for e.g. a first order reaction of chlorine with the wall (Robin BC) (Sookhak Lari *et al.*, 2010). We follow Kader (1981) and define the typical thickness δ_m of the MTBL as the distance from the wall at which $D = D_T$:

$$\delta_m = \sqrt[3]{\frac{Sc_T}{bSc}}\delta_v \tag{2.4}$$

The equation above clearly demonstrates that the MTBL will be nested in the viscous sublayer for $Sc \gg 1$ because $\delta_m/\delta_v \propto Sc^{-1/3}$.

Eqs (2.1) and (2.3) will be used for the asymptotic solutions and are formally only valid very close to the conduit wall. To compare the predictions of the asymptotic solutions to the solutions to the full behaviour of the system, a model which accurately describes u and D_T throughout the entire conduit is required. Over the years, a multitude of models have been developed (see e.g. Reynolds, 1975; Weigand, 2004); here a modified Van Driest mixing-length model has been selected. This turbulence model accurately reproduces the flow and turbulent diffusion in the inner layer, including the cubic dependence of D_T on y very close to the wall. For more details, see Hanna *et al.* (1981); Sookhak Lari *et al.* (2010, 2011).

3. Derivation of far-field equations

Consider the transport of a high Sc solute through a conduit at high Re which exchanges mass with the conduit walls. For fully developed flow through a pipe with radius R, the governing equation is the axisymmetric Reynolds-averaged, steady-state mass transport equation (Bird *et al.*, 2002)

$$u\frac{\partial C}{\partial x} - \frac{1}{r}\frac{\partial}{\partial r}\left[r\left(D + D_T\right)\frac{\partial C}{\partial r}\right] = 0 \tag{3.1}$$

where x and r are the streamwise and radial directions, and $C(x, r)$ is the (Reynolds-averaged) mass concentration. Streamwise diffusion has been neglected,

which is permitted for a flow for which the Péclet number $Pe = ReSc$ is very large. As stated before, we consider a hydrodynamically fully developed flow; u and D_T are therefore functions of r only. The axisymmetric coordinate system is used for convenience of presentation; the approach is equally valid for non-circular cross-sections as long as the viscous wall region ($\propto \delta_v$) is much thinner than the local surface curvature.

Equation (3.1) is supplemented by a wall BC of the form

$$\left.\frac{\partial C}{\partial r}\right|_w = G(C_w) \tag{3.2}$$

where $C_w = C(x, R)$, $\partial C/\partial r|_w = \partial C/\partial r(x, R)$ and $G(C_w)$ is a generic function which depends on the wall concentration. Most BCs can be captured by Eq. (3.2), including the standard (linear) Dirichlet, Neumann and Robin BCs, but also higher order reactions and other BCs for which the wall-flux depends nonlinearly on the wall concentration. We will show that for BCs which satisfy (3.2), the Sherwood number Sh, which is the dimensionless mass flux, is universal and consistent with classical correlations of $Sh(Sc, Re)$. The other two BCs are symmetry in the centre, $\partial C/\partial r|_{r=0} = 0$, and a constant concentration at the entrance: $C(0, r) = C_0$.

For the problem under consideration, the concentration is expected to be uniform, except within the MTBL. A dimensional analysis of the advective and diffusive terms of eq. (3.1) in the MTBL results in

$$u\frac{\partial C}{\partial x} \propto u_\tau \frac{\delta_m}{\delta_v}\frac{\mathcal{C}}{\mathcal{L}}, \qquad \frac{1}{r}\frac{\partial}{\partial r}\left[r\left(D + D_T\right)\frac{\partial C}{\partial r}\right] \propto \frac{1}{R}\frac{RD\mathcal{C}}{\delta_m^2} \tag{3.3}$$

where $\mathcal{C}$ is a typical concentration and $\mathcal{L}$ is the typical length-scale for the streamwise variations. The typical velocity in the MTBL was estimated by evaluating Eq. (2.1) at $y = \delta_m$.

The central premise of the approximation is that streamwise variations occur on much longer lengthscales than changes in the wall-normal direction, i.e. that $\mathcal{L} \gg R$ (Sookhak Lari *et al.*, 2010; Garcia-Ybarra & Pinelli, 2006; Notter & Sleicher, 1972). It follows from the estimates above that advection will be negligible relative to diffusion if the ratio $R/\mathcal{L}$ satisfies

$$\frac{R}{\mathcal{L}} \ll bRe_\tau \tag{3.4}$$

where $Re_\tau = u_\tau R/\nu$ is the shear Reynolds number. The validity of this assumption will be established at the end of this section.

When (3.4) holds, Eq. (3.1) will no longer depend on x. Indeed, by neglecting the advective term, changing coordinates to mass transfer wall units $\eta = (R - r)/\delta_m$, assuming that $\delta_m \ll R$, and using the cubic for D_T given in (2.3), the following linear partial differential equation is obtained

$$\frac{\partial}{\partial \eta}\left[(1 + \eta^3)\frac{\partial c}{\partial \eta}\right] = 0 \tag{3.5}$$

where $c = C/C_0$. The equation above is equivalent to Garcia-Ybarra & Pinelli (2006, eq. 30) and Sookhak Lari *et al.* (2010, eq. 29). One BC is provided by Eq. (3.2) which in dimensionless form is given by

$$\left.\frac{\partial c}{\partial \eta}\right|_w = g(c_w) \tag{3.6}$$

where $g = \delta_m G/C_0$. The second BC used is $c(\xi, \eta \to \infty) = c_b(\xi)$, which states that c tends to the bulk concentration c_b far away from the MTBL. Here, the dimensionless streamwise coordinate ξ is defined as $\xi = x/\mathcal{L}$. With these BCs, Eq. (3.5) admits the following closed-form solution (Garcia-Ybarra & Pinelli, 2006; Sookhak Lari *et al.*, 2010)

$$c(\xi, \eta) = c_b + (c_b - c_w)F(\eta) \tag{3.7}$$

where the wall concentration $c_w(\xi)$ and $F(\eta)$ are defined as

$$F(\eta) = \frac{\sqrt{3}}{2\pi}\left(\log\frac{\eta+1}{\sqrt{\eta^2-\eta+1}} - \sqrt{3}\left(\frac{\pi}{2} - \arctan\frac{2\eta-1}{\sqrt{3}}\right)\right) \tag{3.8}$$

$$c_w = c_b - \frac{g(c_w)}{F'(0)} \tag{3.9}$$

The function F increases monotonically from $F(0) = -1$ to $F(\infty) = 0$, and $F'(0) = 9/(2\pi\sqrt{3})$.

To complete the approximation, an equation is required which governs the behavior of c_b. Such an equation can be obtained by averaging Eq. (3.1) over the cross-section

$$\frac{\mathrm{d}}{\mathrm{d}x}\langle uc\rangle - \frac{D}{r_h}\left.\frac{\partial c}{\partial r}\right|_w = 0 \tag{3.10}$$

where $\langle uc\rangle = \int_0^R rucdr / \int_0^R rdr = \frac{2}{R^2}\int_0^R rucdr$ is the average streamwise mass flux. Because c is assumed constant throughout the cross-section except in the MTBL, we can approximate $\langle uc\rangle \approx Uc_b$, where U is the average velocity. This results in

$$U\frac{\mathrm{d}c_b}{\mathrm{d}x} + \frac{J_w}{r_h} = 0 \tag{3.11}$$

where $r_h = R/2$ is the hydraulic radius and J_w is the wall mass flux per unit area

$$J_w = -D\left.\frac{\partial C}{\partial r}\right|_w = \frac{DC_0}{\delta_m}\left.\frac{\partial c}{\partial \eta}\right|_w \tag{3.12}$$

Substituting Eq. (3.12) into (3.11) results in

$$\frac{\mathrm{d}c_b}{\mathrm{d}\xi} + \left.\frac{\partial c}{\partial \eta}\right|_w = 0 \tag{3.13}$$

and

$$\mathcal{L} = r_h\frac{U\delta_m}{D} = \frac{r_h}{2}\frac{ReSc^{2/3}Sc_T^{1/3}}{Re_\tau b^{1/3}} \tag{3.14}$$

Here, we have used the standard pipe Reynolds number definition $Re = 2UR/\nu$. The typical lengthscale $\mathcal{L}$ can be interpreted as the distance for which the

solute mass in the entire cross-section is depleted by the flux through the wall. Eq. (3.14) can be used to check the validity condition (3.4), which now takes the form of $b^{2/3}ReSc^{2/3} \gg 1$. Even for very low values of $Re = 2000$ and $Sc = 100$, $b^{2/3}ReSc^{2/3} \approx 466$ and therefore, condition (3.4) is satisfied for high Sc compounds in turbulent flows.

Eqs (3.7), (3.9) and (3.13) comprise a set of coupled equations which can be used to construct asymptotic far-field solutions for the concentration profile and the mass transfer at the wall. Because the derivation does not rely on linear techniques such as separating variables, this includes nonlinear BCs. Examples will be discussed §5.

4. A universal Sherwood number equation

A universal expression for the Sherwood number Sh can be derived for BCs satisfying Eq. (3.6). The Sherwood number is defined by $Sh = 2k_f R/D$, where k_f $[LT^{-1}]$ is the mass transfer coefficient (Bird *et al.*, 2002)

$$k_f = \frac{J_w}{C_b - C_w} \tag{4.1}$$

Substituting Eq. (3.9) into Eq. (4.1), and using that $J_w = g(c_w)DC_0/\delta_m$ results in

$$k_f = \frac{9}{2\pi\sqrt{3}}\frac{D}{\delta_m} \tag{4.2}$$

i.e. k_f is *independent* of the type of BC. Using Eq. (4.2), the Sh equation for high Sc compounds is

$$Sh = \frac{9b^{1/3}}{\pi\sqrt{3}Sc_T^{1/3}}Re_\tau Sc^{1/3} \tag{4.3}$$

The universality is a direct consequence of the linear dependence of the wall concentration gradient and the concentration difference between wall and bulk, as is evident from (3.9). The underlying reason for this is the invariance of (3.5) to scaling because of its linearity.

The universality of Eq. (4.3) is confirmed by recent work with Robin BCs (Sookhak Lari *et al.*, 2010) and Dirichlet BCs (Garcia-Ybarra & Pinelli, 2006). It also compares favourably with experimental data. The Fanning friction factor f is defined as $f = 2\tau_w/(\rho U^2) = 8Re_\tau^2/Re^2$ (Bird *et al.*, 2002, Eq. 6.1-4a). Substitution into Eq. (4.3) results in

$$Sh = \frac{9b^{1/3}}{\pi\sqrt{24}Sc_T^{1/3}}\sqrt{f}ReSc^{1/3} \tag{4.4}$$

which corresponds well to the established correlation $Sh = 0.0566\sqrt{f}ReSc^{1/3}$ (Bird *et al.*, 2002, Eq. 14.2-5) upon substituting $b = 9.5 \times 10^{-4}$ and $Sc_T = 1$. By applying the Blasius formula $f = 0.0791\ Re^{-0.25}$ (Bird *et al.*, 2002, Eq. 6.2-12), we

obtain $Sh = 0.016 Re^{0.88} Sc^{1/3}$ which is in good agreement with the Sh correlations presented in the supplementary material.

The Stanton number St is defined as the ratio of mass transfer coefficient to average velocity:

$$St = \frac{k_f}{U} = \frac{Sh}{ReSc} = \frac{9b^{1/3}}{\pi\sqrt{24}Sc_T^{1/3}}\sqrt{f}Sc^{-2/3} \tag{4.5}$$

Note that St is closely related to $\mathcal{L}$ by $\mathcal{L}/2R = 9/(8\pi\sqrt{3}St)$. The value of St will therefore immediately give an indication of the appropriateness of neglecting the streamwise advection.

5. Far-field solutions

(*a*) *Linear BCs*

We will now provide closed-form far-field solutions for Dirichlet, Neumann, and Robin BCs, by considering a linear BC of the form

$$\alpha c_w + \beta \left.\frac{\partial c}{\partial \eta}\right|_w = \gamma \tag{5.1}$$

Here, α, β and γ are constants. Using Eqs (3.6), (3.9) and (5.1), the wall concentration and gradient are given by

$$c_w = \frac{\beta c_b - \frac{2\pi\sqrt{3}}{9}\gamma}{\beta - \frac{2\pi\sqrt{3}}{9}\alpha}, \qquad \left.\frac{\partial c}{\partial \eta}\right|_w = \frac{\gamma}{\beta} - \frac{\alpha}{\beta}c_w \tag{5.2}$$

Substituting (5.2) into (3.13) and solving for c_b results in

$$c_b = \frac{\gamma}{\alpha} + \left(1 - \frac{\gamma}{\alpha}\right)\exp\left(-\frac{\alpha}{-\beta + \frac{2\pi\sqrt{3}}{9}\alpha}\xi\right) \tag{5.3}$$

The specific solutions for Dirichlet ($\alpha = 1$, $\beta = 0$), Neumann ($\alpha = 0$ and $\beta = 1$) and Robin ($\alpha = -\sigma$, $\beta = 1$ and $\gamma = 0$) BCs are presented in table 1 as solution AS-D, AS-N and AS-R, respectively. The Neumann solution required performing a Taylor series expansion around $\xi = 0$ and taking the limit of $\alpha \to 0$. Solution AS-R is equivalent to the solution derived in Sookhak Lari *et al.* (2010). AS-N is documented to a large extent in Bird *et al.* (2002), pp411-414, but that solution still contains an integral which needs to be approximated numerically. Garcia-Ybarra & Pinelli (2006) derived $F(\eta)$ and (4.5) for Dirichlet BCs, but did not solve for c_b (solution AS-D).

The far-field asymptotic solutions (AS) will be compared to solutions of Eq. (3.1) obtained with the method of separating variables (SV). To allow comparison to the full solution, the SV method retains the cylindrical coordinate system and uses the realistic velocity and diffusivity profiles provided by the modified Van Driest Mixing length model. An expansion of the form

	$c(\xi,\eta)$	$\dfrac{c-c_w}{c_b-c_w}$
AS-D	$\gamma+(1-\gamma)\exp\left(-\dfrac{9}{2\pi\sqrt{3}}\xi\right)(1+F(\eta))$	$1+F(\eta)$
SV-D	$\gamma+(1-\gamma)\dfrac{Re_m^2}{2}\displaystyle\sum_{n=1}^{\infty}\dfrac{Y_n'(0)}{k_n}\exp(-k_n\xi)Y_n(\eta)$	$\dfrac{Y_1(\eta)}{Y_1(Re_m)}$
AS-N	$1-\gamma\xi+\gamma\dfrac{2\pi\sqrt{3}}{9}F(\eta)$	$1+F(\eta)$
SV-N	$1-\gamma\xi+\dfrac{\gamma Re_m^2}{2}\displaystyle\sum_{n=2}^{\infty}\dfrac{Y_n(0)}{k_n}(\exp(-k_n\xi)-1)Y_n(\eta)$	$\dfrac{\sum_{n=2}^{\infty}\frac{Y_n(0)}{k_n}(Y_n(\eta)-Y_n(0))}{\sum_{n=2}^{\infty}\frac{Y_n(0)}{k_n}(Y_n(Re_m)-Y_n(0))}$
AS-R	$\left(1+\dfrac{\frac{2\pi\sqrt{3}}{9}\sigma}{1+\frac{2\pi\sqrt{3}}{9}\sigma}F(\eta)\right)\exp\left(-\dfrac{\sigma}{1+\frac{2\pi\sqrt{3}}{9}\sigma}\xi\right)$	$1+F(\eta)$
SV-R	$\dfrac{Re_m^2}{2}\displaystyle\sum_{n=1}^{\infty}\dfrac{Y_n'(0)}{k_n}\exp(-k_n\xi)Y_n(\eta)$	$\dfrac{Y_1(\eta)-Y_1(0)}{Y_1(Re_m)-Y_1(0)}$

Table 1. Analytical solutions for Dirichlet, Neumann and Robin BCs using the asymptotic solution (AS) and method of separating variables (SV).

$$c(\xi,\eta)=h(\eta)+\sum_{n=1}^{\infty}X_n(\xi)Y_n(\eta) \tag{5.4}$$

is used, where $h(\eta)$ is a function which maps (5.1) onto a homogeneous BC. The eigenvalues k_n and associated eigenfunctions $Y_n(\eta)$ can be found by solving a Sturm-Liouville problem. The Ordinary Differential Equation (ODE) governing X_n can be solved analytically and takes the form of a damped exponential if $k_n>0$ and a linear function if $k_n=0$. The eigenvalues and eigenfunctions do not have closed-form solutions and are determined numerically using a shooting method. Details of the method and implementation are discussed in the supplementary material.

The solutions for Dirichlet, Neumann and Robin BCs using the method of separating variables are presented in table 1 and are denoted by SV-D, SV-N and SV-R, respectively. The parameter $Re_m=R/\delta_m$ represents the distance to the center of the pipe in mass-transfer units[1]. It is clear from table 1 that the structure of the two solution methods is very similar.

All results presented in this paper are for $Re_\tau=2000$, $Sc=1000$ and $Sc_T=1$ unless stated otherwise. The prediction for AS-D is $k_1=9/(2\pi\sqrt{3})\approx 0.8270$, which compares well with SV-D, which predicts $k_1=0.8510$. For AS-R with $\sigma=2$, $k_1=\sigma/(1+\frac{2\pi\sqrt{3}}{9}\sigma)\approx 0.5851$, against SV-R which predicts $k_1=0.5970$. The small difference can be traced back to differences in the eddy diffusivity profile. The wall damping employed in the modified Van Driest mixing length model is purely empirical, and only satisfies cubic behaviour very close to the wall. Between $1<y^+<5$, D_T is up to thirty percent higher than a pure cubic. This

[1] Note that Re_m is directly related to Sh as $Sh=(9/\pi\sqrt{3})Re_m$.

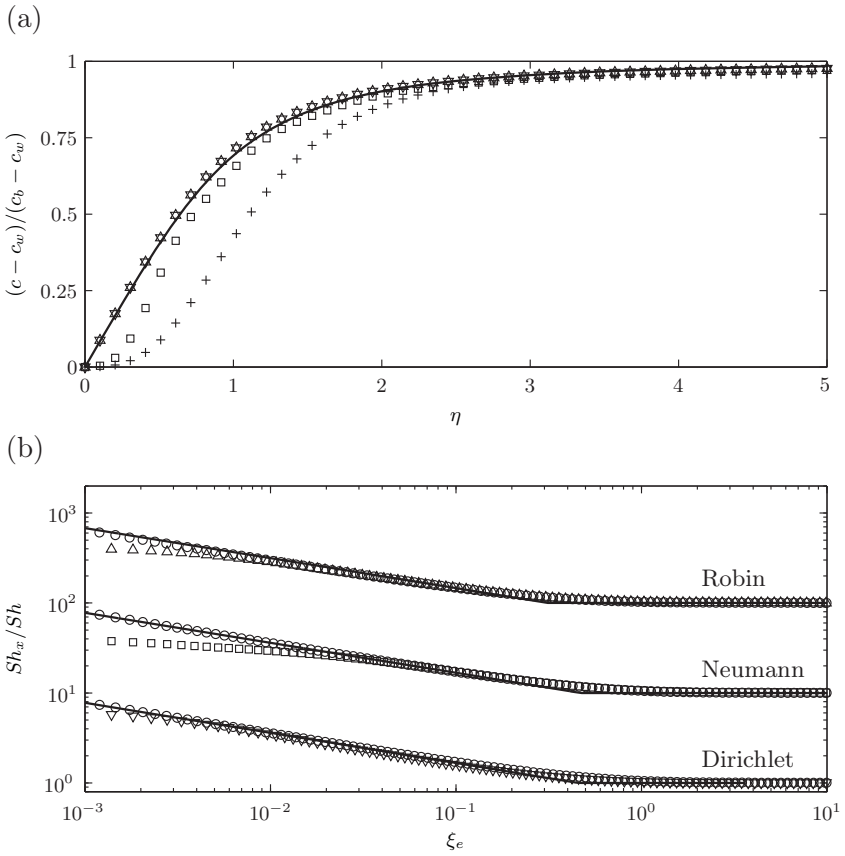

Figure 2. Comparison of asymptotic solutions for linear BCs. (a) far-field solution: $(c-c_w)/(c_b-c_w)$ for various BCs. $1+F$ [——]; SV-D [△]; SV-N ($N=25$) [+]; SV-N ($N=100$) [▫]; SV-R ($\sigma=2$) [▽]. (b) near-field solution: Sh_x for Dirichlet (Sh_x multiplied by 100), Neumann (Sh_x multiplied by 10) and Robin BCs. 3D axi-symmetric simulations [○] and the other symbols as before.

will make the MTBL a bit thinner, which in return results in a slightly higher decay coefficient. This small difference could have been avoided altogether by adopting a modified value for b/Sc_T using the calculation method outlined in appendix 1, but presenting the slight differences was deemed more instructive.

It is clear from (3.7) that $(c-c_w)/(c_b-c_w)=1+F(\eta)$ regardless of the BC. For the method of separating variables, $(c-c_w)/(c_b-c_w)$ in the far-field can be obtained by setting $\exp(-k_n\xi)\approx 0 \quad \forall \quad n=2,3,\ldots$. The equations are presented in the third column of table 1 and are plotted in Fig. 2(a). For SV-D and SV-R, $(c-c_w)/(c_b-c_w)$ is closely related to the first eigenfunction and the correspondence to the far-field asymptotic solution is excellent. The small differences originate again from the differences in turbulence model, and could be avoided using a modified value for b/Sc_T (appendix 1). For SV-N, $(c-c_w)/(c_b-c_w)$ shows deviations very close to the wall which are caused by a truncation of the infinite sum. The convergence to the asymptotic solution can

be seen to be quite slow as is evident from the profile for $N = 25$ modes [+] and $N = 100$ modes [▫].

(*b*) *Nonlinear BCs*

Approximate analytical solutions can be constructed for nonlinear BCs. As a demonstration, a second-order wall reaction

$$\left.\frac{\partial c}{\partial \eta}\right|_w = \frac{9}{4\pi\sqrt{3}} a c_w^2 \tag{5.5}$$

is studied, where a is a dimensionless reaction coefficient. Substituting (5.5) into (3.9) gives

$$c_w = a^{-1}\left(\sqrt{1+2ac_b}-1\right) \tag{5.6}$$

Substitution of (5.6) and (5.5) into (3.13) results in

$$\frac{\mathrm{d}c_b}{\mathrm{d}\xi} + \frac{9}{4\pi\sqrt{3}} \frac{\left(\sqrt{1+2ac_b}-1\right)^2}{a} = 0 \tag{5.7}$$

The change of variables $\phi = (\sqrt{1+2ac_b}-1)^{-1}$ simplifies Eq. (5.7) to

$$\frac{\phi+1}{\phi}\frac{\mathrm{d}\phi}{\mathrm{d}\xi} - \frac{9}{4\pi\sqrt{3}} = 0 \tag{5.8}$$

which has a solution

$$\phi = W_0\left(\exp\left(\frac{9}{4\pi\sqrt{3}}\xi + A\right)\right) \tag{5.9}$$

where $A = \phi_0 + \log\phi_0$, $\phi_0 = \left(\sqrt{1+2a}-1\right)^{-1}$ and W_0 is the Lambert W function (Corless *et al.*, 1996).

The far-field asymptotic solution in Eq. (5.9) was compared to the solution of a finite-volume approximation of the full 3D-axisymmetric partial differential equation (3.1) and mass transfer BC (5.5). As for the method of separating variables, the modified Van Driest mixing-length model was used to determine velocity and turbulent diffusivity profiles. The advective term was discretised using a first-order upwind scheme, which allows for explicit marching in the x-direction. The r-direction is discretised using second order central scheme which is solved using direct matrix inversion. The nonlinearity of the BC (5.5) is incorporated using a simple iterative method.

The problem was solved for $a = 10^{-1}$, 10^0 and 10^1. Grid convergence was observed at $N_x = 1200$ and $N_r = 600$, although logarithmic spacing was required because of strong variations very close to the wall and near the entrance. The cell-sizes vary up to eight orders of magnitude. A conservative method such as the finite volume method is crucial for such extreme stretching (Mathias & van Reeuwijk, 2009). The Grid Convergence Index (GCI, see Roache, 1994) for these simulations is GCI < 1.2 % in the far-field based on $c_b(\mathcal{L})$. Note that in the calculation of the GCI we assumed that the method is entirely first order; the reported value for the GCI is therefore a conservative estimate.

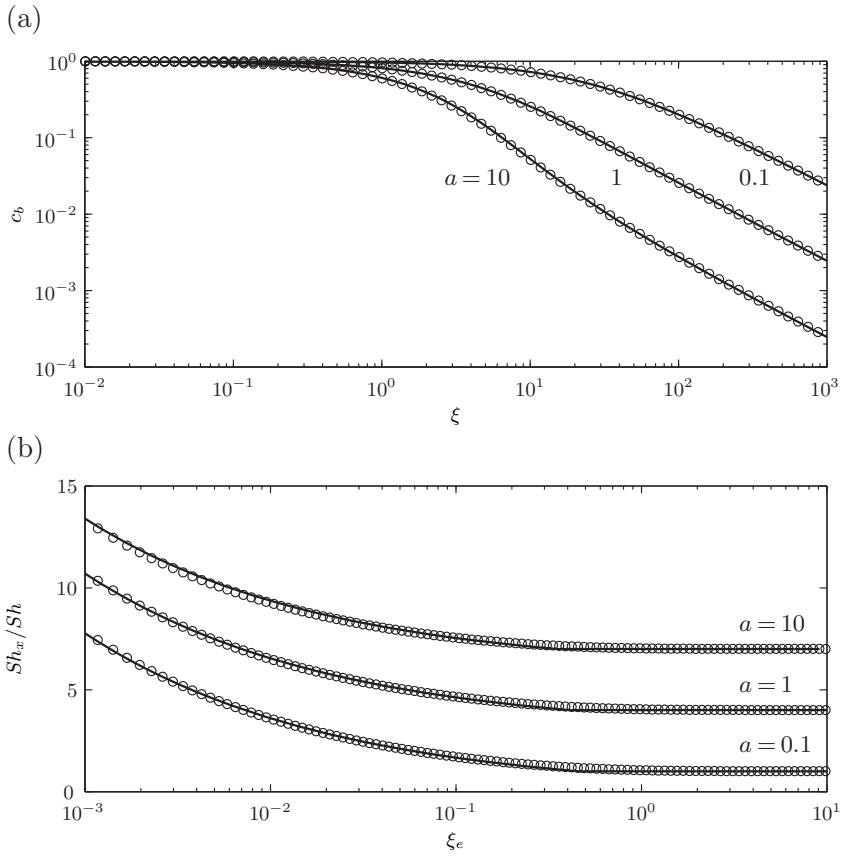

Figure 3. Comparison of the asymptotic solution [——] with the numerical solution [○] for the nonlinear BC (5.5). (a) far-field solution for $a = 0.1$, 1, and 10. (b) near-field solution for $a = 10$ (Sh_x shifted by 6), $a = 1$ (Sh_x shifted by 3) and $a = 0.1$.

The asymptotic solution for c_b (5.9) and the 3D-axisymmetric simulations are in excellent agreement (Fig. 3(a)), even though the asymptotic solution does not take into account entrance effects. In the next section, we will show that this is the case because the entrance length $\mathcal{L}_e$ is so small that it does not influence c_b.

6. Near-field solutions

In the near-field, streamwise advection will not be negligible. In dimensionless variables, (3.1) is given by

$$\epsilon\eta\frac{\partial c}{\partial \xi} - \frac{\partial}{\partial \eta}\left[(1+\eta^3)\frac{\partial c}{\partial \eta}\right] = 0 \tag{6.1}$$

Here, (2.1), (2.3) were used for the velocity and eddy diffusivity profiles, respectively. The small parameter ϵ is given by

$$\epsilon = \frac{u_\tau \delta_m^2}{\delta_v r_h U} = 4 \left(\frac{Sc_T}{b} \right)^{2/3} Re^{-1} Sc^{-2/3} \tag{6.2}$$

Hence, a suitable near-field coordinate is $\xi_e = \xi/\epsilon$, for which (6.1), (3.13) become

$$\eta \frac{\partial c}{\partial \xi_e} - \frac{\partial}{\partial \eta} \left[(1+\eta^3) \frac{\partial c}{\partial \eta} \right] = 0 \tag{6.3}$$

$$\frac{\mathrm{d}c_b}{\mathrm{d}\xi_e} + \epsilon \left. \frac{\partial c}{\partial \eta} \right|_w = 0 \tag{6.4}$$

The equations above are parameter-free which suggests universal behaviour, although it should be noted that the BCs may still introduce a parameter dependence. As $\epsilon \ll 1$, (6.4) immediately results in $c_b(\xi_e) \approx 1$. The entrance lengthscale $\mathcal{L}_e$ is given by

$$\mathcal{L}_e = \epsilon \mathcal{L} = \frac{Sc_T}{bRe_\tau} R \tag{6.5}$$

Note that $\mathcal{L}_e$ depends on flow properties only. This can be understood by realising that $\mathcal{L}_e$ is related to the time T_D it takes for the mass in the MTBL to deplete: $T_D \propto C\delta_m/J_w \approx C\delta_m/(DC/\delta_m) = \delta_m^2/D$. During this time, the boundary layer section moves at a typical velocity $\delta_m/\delta_v u_\tau$, which is the velocity at the edge of the MTBL. The entrance lengthscale $\mathcal{L}_e$ can therefore be estimated by

$$\mathcal{L}_e \propto \frac{\delta_m}{\delta_v} u_\tau \frac{\delta_m^2}{D} = \frac{\delta_v}{b} = \frac{1}{bRe_\tau} R \tag{6.6}$$

Note that the validity condition (3.4) for the approximation can be expressed using $\mathcal{L}_e$ and $\mathcal{L}$ as

$$\frac{\mathcal{L}_e}{\mathcal{L}} = \epsilon \ll 1 \tag{6.7}$$

In order to obtain closed form solutions for (6.3), the Von Karman-Pohlhausen integral method (Lighthill, 1950; Spalding, 1954; Schlichting & Gersten, 2000) will be used. This method is not exact as it involves substituting the assumed concentration profile $F(\eta)$. However, (6.3) does not admit self-similar solutions, because 1) the BC (3.6) is nonlinear and 2) the total diffusion $(1+\eta^3)$ does not allow powerlaw behaviour for the boundary layer thickness.

By introducing the concentration deficit

$$\Delta(\xi_e, \eta) = c_b(\xi_e) - c(\xi_e, \eta) = 1 - c(\xi_e, \eta) \tag{6.8}$$

and integrating from $\eta = 0$ to $\lambda\delta(\xi)$, (6.3) becomes

$$\frac{\mathrm{d}}{\mathrm{d}\xi_e} \int_0^{\lambda\delta} \eta \Delta d\eta + \left. \frac{\partial \Delta}{\partial \eta} \right|_w = 0 \tag{6.9}$$

here, $\delta(\xi)$ is the typical boundary layer thickness and $\lambda > 1$ is a coefficient.

BC	g'	Solution
Dirichlet	$\pm\infty$	$\delta = \left(\frac{3F'(0)}{2B}\xi_e\right)^{1/3}$
Neumann	0	$\delta = \left(\frac{F'(0)}{B}\xi_e\right)^{1/3}$
Robin	σ	$\frac{2}{3}\delta^3 + \frac{F'(0)}{2\sigma}\delta^2 - \frac{F'(0)^2}{\sigma^2}\delta - \frac{F'(0)^3}{\sigma^3}\log\left(\frac{1}{1+\frac{\sigma}{F'(0)}\delta}\right) = \frac{F'(0)}{B}\xi_e$

Table 2. Near-field solution for boundary layer thickness δ for Dirichlet, Neumann and Robin BCs.

The concentration is assumed to be of the form $c(\xi_e, \zeta) = c_b + (c_b - c_w)F(\zeta)$ where $\zeta = \eta/\delta$. In terms of the concentration deficit, the assumed profile is

$$\Delta(\xi_e, \zeta) = -\Delta_w(\xi_e)F(\zeta) \tag{6.10}$$

By substituting (6.10) into (6.9) and changing variables to ζ, we obtain

$$2B\delta\Delta_w\delta' + \delta^2 B\Delta_w' = F'(0)\frac{\Delta_w}{\delta} \tag{6.11}$$

where

$$B = -\int_0^\lambda \zeta F(\zeta)d\zeta \tag{6.12}$$

Combining (3.6) and (6.10) results in

$$\Delta_w = \frac{\delta g(c_w)}{F'(0)} \tag{6.13}$$

and substituting the expression above into (6.11) finally yields

$$\left(2 + \frac{1}{1+\frac{1}{F'(0)}g'\delta}\right)\delta^2\delta' = \frac{F'(0)}{B} \tag{6.14}$$

Equation (6.14) is a first order nonlinear ODE. For the general BC (3.6), $g' = g'(c_w)$ which therefore introduces another dependence on δ. It may therefore be impossible to derive closed-form solutions for complicated BCs. For the linear BC (5.1) however, $g' = -\alpha/\beta$ evaluates to a constant. In table 2, the solutions to (6.14) are presented for Dirichlet ($\alpha = 1$, $\beta = 0$), Neumann ($\alpha = 0$, $\beta = 1$) and Robin ($\alpha = -\sigma$, $\beta = 1$, $\gamma = 0$) BCs. The Dirichlet and Neumann BCs have the classic $x^{1/3}$ dependence (Linton & Sherwood, 1950; Kestin & Persen, 1962; Shaw *et al.*, 1963; Berger & Hau, 1977). The Robin BC is more complex because g' is finite, but essentially behaves like a Neumann BC when $\sigma \ll 1$ and like a Dirichlet BC when $\sigma \gg 1$.

Although the Sh correlation for the far-field is the same for all BCs satisfying (3.6), the near-field correlation $Sh_x(\xi_e)$ is different. Indeed, the mass transfer coefficient is given by $k_f = DF'(0)/(\delta_m\delta)$ and therefore

$$\frac{Sh_x}{Sh} = \frac{1}{\delta} \tag{6.15}$$

The coefficient λ controls, via B, the growth rate of the boundary layer. As the integral (6.12) is divergent for $\lambda \to \infty$, λ has to be tuned to results from 3D-axisymmetric simulations of the full problem. The resolution of the simulations is $N_x = 1200$ and $N_r = 600$ and the GCI < 1 % based on $c_b(\mathcal{L})$. Good agreement is found for $\lambda = 1.5$ and therefore $B = 0.4$. The near-field and far-field solutions can be combined using $Sh_x/Sh = \max(\delta^{-1}, 1)$. The correspondence of the equation for Sh_x with 3D-axisymmetric solutions for Dirichlet, Neumann and Robin BCs is good (Fig. 2(b)). Note that Sh_x for the Dirichlet and Neumann BCs are scaled by a factor 100 and 10, respectively. Also shown are the solutions obtained using the method of separating variables using the first 100 modes. There is good agreement with both the asymptotic solutions and the simulations, although more modes are required to describe the behaviour for $\xi_e < 10^{-2}$.

Using the same substitutions as for the Sh correlation, the Sh_x correlation for Dirichlet BCs is given by

$$Sh_x = 0.19 Re^{0.58} Sc^{1/3} \left(\frac{x}{2R}\right)^{-1/3} \tag{6.16}$$

This correlation is in good agreement with electrochemical mass transfer experiments which report $Sh_x = 0.184 Re^{0.58} Sc^{1/3} (x/2R)^{-1/3}$ (Shaw *et al.*, 1963; Berger & Hau, 1977)[2]. For the asymptotic solution for Neumann BCs, the correlation is identical to (6.16) but the prefactor is 0.22.

For nonlinear BCs, g' depends on c_w. For the second order wall reaction (5.5), substitution into (6.13) results in a quadratic in Δ_w, of which the physically relevant root is given by

$$\Delta_w = \frac{1 + a\delta - \sqrt{1 + 2a\delta}}{a\delta} \tag{6.17}$$

Therefore, g' is given by

$$g' = F'(0) \frac{\sqrt{1 + 2a\delta} - 1}{\delta} \tag{6.18}$$

Substitution of the equation above into (6.14) and solving the ODE results in

$$\frac{2}{3}\delta^3 + \frac{(1 + 2a\delta)^{5/2}}{20a^3} - \frac{(1 + 2a\delta)^{3/2}}{6a^3} + \frac{(1 + 2a\delta)^{1/2}}{4a^3} - \frac{2}{15a^3} = \frac{F'(0)}{B}\xi_e \tag{6.19}$$

The good agreement of Sh_x/Sh based on the equation above with the numerical simulation is shown in Fig. 3(b) for three different values of a. Note that B was kept the same value as for the linear BCs.

[2] The experiments report the average Sherwood number over the interval 0 to x, which implies a conversion factor of 3/2.

7. Concluding remarks

In this paper, asymptotic solutions for high Sc scalars for both linear and nonlinear BCs were developed, which provide simple closed-form solutions and predict accurately the concentration profile and mass transfer in the near- and the far-field. It was shown that in the far-field, the mass transfer coefficient k_f and associated dimensionless Sherwood number Sh is *independent* of the specific wall BC. This result is valid for all BCs satisfying (3.6), which include virtually all known BCs including those of Dirichlet, Neumann and Robin type. This is a remarkable result which emphasises that for high Sc turbulent flows, the mass transfer coefficient k_f (4.2) depends only on the molecular diffusivity D and the thickness of the mass transfer boundary layer δ_m.

The method presented in this paper assumed that the eddy diffusivity D_T is a cubic in the distance to the wall. As discussed in §2, the precise near-wall behaviour of D_T is subject to some uncertainty. However, the universality of the mass transfer coefficient is independent of the exact profile for D_T. Indeed, making use of a different profile for D_T, for example the fourth order polynomial suggested in Garcia-Ybarra (2009), would have lead to the same conclusion.

The solutions reported in this paper can be used even when the actual D_T profile is not cubic by calculating the effective value for b/Sc_T using the procedure described in the appendix. This procedure matches δ_m from the actual D_T profile to that of the assumed cubic, thereby ensuring that the integral parameters are predicted accurately. Note that this would make the parameter b/Sc_T dependent on Re and Sc. As discussed in §2, the D_T profile may be different for specific BCs. In that case, b/Sc_T would have a different Sc and Re dependence for each BC and therefore the Sh correlation (4.3) would not be universal. It is therefore desirable that further research focusses on the near-wall profile of D_T at high Sc turbulent mass transfer, in particular the influence of different BCs.

Inferring the value of b/Sc_T from turbulence models

The coefficient b has a strictly defined physical meaning stated in (2.2). However, it can also be treated as a free parameter representing a measure for the "conductivity" of the MTBL, in which case the value can be determined from the turbulence model employed. We start from (3.1), neglect horizontal advection and change to plus-units using the change of variables $r = \delta_v(Re_\tau - y^+)$. The result is

$$\frac{\partial}{\partial y^+}\left[\left(1+\frac{D_T}{D}\right)\frac{\partial C}{\partial y^+}\right]=0 \tag{A.1}$$

Integrating twice and using (3.2) results in

$$C_b - C_w = \delta_v G(C_w)\int_0^{Re_\tau}\frac{1}{1+ScD_T/\nu}dy^+ \tag{A.2}$$

and the mass transfer coefficient k_f is therefore given by

$$k_f = \frac{D}{\delta_v}\left[\int_0^{Re_\tau} \frac{1}{1 + ScD_T/\nu} dy^+\right]^{-1} \tag{A.3}$$

Many theoretical studies on mass transfer approximate the integral on the right hand side to develop Sh correlations (e.g. Kader & Yaglom, 1972; Aravinth, 2000).

By equating the equation above to (4.2) and using (2.4), we obtain

$$\left(\frac{b}{Sc_T}\right)^{1/3} = \frac{2\pi\sqrt{3}}{9}\left[\int_0^{Re_\tau} \frac{Sc^{1/3}}{1 + Sc\frac{D_T}{\nu}} dy^+\right]^{-1} \tag{A.4}$$

which allows for the calculation of an effective conductivity parameter b/Sc_T for each given turbulence model.

References

Al-Jasser, A. 2007 Chlorine decay in drinking-water transmission and distribution systems: Pipe service age effect. *Water Res.* **41**, 387–396.

Antonia, R. A. & Kim, J. 1991 Turbulent Prandtl number in the near-wall region of a turbulent channel flow. *Int. J. Heat Mass Tran.* **34** (7), 1905–1908.

Aravinth, S. 2000 Prediction of heat and mass transfer for fully developed turbulent fluid flow through tubes. *Int. J. Heat Mass Tran.* **43** (8), 1399–1408.

Bergant, R. & Tiselj, I. 2007 Near-wall passive scalar transport at high Prandtl numbers. *Phys. Fluids* **19** (6), 065105.

Berger, F. P. & Hau, K. F. F. L. 1977 Mass-transfer in turbulent pipe-flow measured by electrochemical method. *Int. J. Heat Mass Tran.* **20** (11), 1185–1194.

Bergmann, J. & Fiebig, M. 1999 Comparison of experimental and numerical investigation on local and global heat transfer in turbulent square channel flow with roughness elements in the form of V-shaped broken ribs. *Flow Turbul. Combust.* **62**, 163–181.

Bird, R., Stewart, W. & Lightfoot, E. 2002 *Transport Phenomena* 2^{nd} *Ed.*. John Wiley and Sons.

Biswas, P., Lu, C. & Clark, R. 1993 A model for chlorine concentration decay in pipes. *Water Res.* **27**, 1715–1724.

Clark, R. M. & Haught, R. C. 2005 Characterizing pipe wall demand: Implication of water quality modeling. *J. Water Res. Pl.-ASCE* **131**, 208–217.

Corless, R. M., Gonnet, G. H., Hare, D. E. G., Jeffrey, D. J. & Knuth, D. E. 1996 On the Lambert W function. *Adv. Comput. Math.* **5**, 329–359.

Crimaldi, J. P., Kossef, J. R. & Monismith, S. G. 2006 A mixing-length formulation for the turbulent Prandtl number in wall-bounded flows with bed roughness and elevated scalar sources. *Phys. Fluids* **18** (8), 095102.

Dawson, D. A. & Trass, O. 1972 Mass-transfer at rough surfaces. *Int. J. Heat Mass Tran.* **15** (7), 1317–1336.

Garcia-Ybarra, P. I. & Pinelli, A. 2006 Turbulent channel flow concentration profile and wall deposition of a large Schmidt number passive scalar. *C. R. Mechanique* **334** (334), 531–538.

Garcia-Ybarra, P. L. 2009 Near-wall turbulent transport of large-Schmidt-number passive scalars. *Phys. Rev. E* **79**, 067302.

Hanna, O. T., Sandall, O. C. & Mazet, P. R. 1981 Heat and mass transfer in turbulent flow under conditions of drag reduction. *AIChE J.* **27**, 693–697.

Harriott, P. & Hamilton, R. 1965 Solid-liquid mass transfer in turbulent pipe flow. *Chem. Eng. Sci.* **20**, 1073–1078.

Kader, B. A. 1981 Temperature and concentration profiles in fully turbulent boundary-layers. *Int. J. Heat Mass Tran.* **24** (9), 1541–1544.

Kader, B. A. & Yaglom, A. M. 1972 Heat and mass-transfer laws for fully turbulent wall flows. *Int. J. Heat Mass Tran.* **15** (12), 2329–2351.

Kawamura, H., Ohsaka, K., Abe, H. & Yamamoto, K. 1998 DNS of turbulent heat transfer in channel flow with low to medium-high Prandtl number fluid. *Int. J. Heat Fluid Fl.* **19** (5), 482–491.

Kestin, J. & Persen, L. 1962 The transfer of heat across a turbulent boundary layer at very high Prandtl numbers. *Int. J. Heat Mass Tran.* **5**, 355–371.

Kozuka, M., Seki, Y. & Kawamura, H. 2009 DNS of turbulent heat transfer in a channel flow with a high spatial resolution. *Int. J. Heat Fluid Fl.* **30** (3), 514–524.

Lévêque, M. A. 1928 Les lois de la transmission de chaleur par convection. *Ann. Mines Memories* **12–13**, 201–299, 305–362, 381–415.

Lighthill, M. 1950 Contributions to the theory of heat transfer through a laminar boundary layer. *Proc. R. Soc. A* **202**, 350–377.

Linton, W. & Sherwood, T. 1950 Mass transfer from solid shapes to water in streamline and turbulent flow. *Chem. Eng. Progr.* **46**, 248.

Mathias, S. A. & van Reeuwijk, M. 2009 Hydraulic fracture propagation with 3-D leak-off. *Transport Porous Med.* **80** (3), 499–518.

Mizushina, T., Ogino, F., Oka, Y. & Fukuda, H. 1971 Turbulent heat and mass transfer between wall and fluid streams of large Prandtl and Schmidt numbers. *Int. J. Heat Mass Tran.* **14** (10), 1705–&.

Munavalli, G. R. & Mohan Kumar, M. 2004 Dynamic simulation of multicomponent reaction transport in water distribution systems. *Water Res.* **38**, 1971–1988.

Na, Y. & Hanratty, T. J. 2000 Limiting behavior of turbulent scalar transport close to a wall. *Int. J. Heat Mass Tran.* **43** (10), 1749–1758.

Noguera, D. & Morgenorth, E. 2004 Introduction to the IWA task group on biofilm modelling. *Water Sci. Technol.* **49**, 131–136.

Notter, R. H. & Sleicher, C. A. 1971 Solution to turbulent Graetz problem by matched asymptotic expansions. 2. case of uniform wall heat flux. *Chem. Eng. Sci.* **26** (4), 559.

Notter, R. H. & Sleicher, C. A. 1972 Solution to turbulent Graetz problem. 3. fully developed and entry region heat-transfer rates. *Chem. Eng. Sci.* **27** (11), 2073.

Pope, S. 2000 *Turbulent Flows*. Cambridge University Press.

Reynolds, A. J. 1975 Prediction of turbulent Prandtl and Schmidt numbers. *Int. J. Heat Mass Tran.* **18** (9), 1055–1069.

Roache, P. 1994 Perspective: a method for uniform reporting of grid refinement studies. *J. Fluid Eng.-T. ASME* **116**, 405–413.

Rossman, L. A., Clark, R. M. & Grayman, W. 1994 Modelling chlorine residuals in drinking water distribution systems. *J. Environ. Eng.-ASCE* **120**, 803–820.

Sarin, P., Snoeyink, D. A., Lytle, D. & Kriven, W. M. 2004 Iron corrosion scales; model for scale growth, iron release and colored water formation. *J. Environ. Eng.-ASCE* **130**, 364–373.

Schlichting, H. & Gersten, K. 2000 *Boundary layer theory*. McGraw-Hill.

Schwertfirm, F. & Manhart, M. 2007 DNS of passive scalar transport in turbulent channel flow at high Schmidt numbers. *Int. J. Heat Fluid Fl.* **28** (6), 1204–1214.

Shaw, D. & Hanratty 1977 Turbulent mass transfer rates to a wall at high Schmidt number. *AlChE J.* **23**, 28–37.

Shaw, P., Reiss, L. & Hanra 1963 Rates of turbulent transfer to a pipe wall in the mass transfer entry region. *AIChE J.* **9**, 362–364.

Sleicher, C. A., Notter, R. H. & Crippen, M. D. 1970 A solution to turbulent Graetz problem by matched asymptotic expansions. 1. case of uniform wall temperature. *Chem. Eng. Sci.* **25** (5), 845.

Sookhak Lari, K., van Reeuwijk, M. & Maksimović, C. 2010 Simplified numerical and analytical approach for solutes in turbulent flow reacting with smooth pipe walls. *J. Hydraul. Eng.-ASCE* **136**, 626–632.

Sookhak Lari, K., van Reeuwijk, M., Maksimović, v. & Sharifan, S. 2011 Combined bulk and wall reactions in turbulent pipe flow: decay coefficients and concentration profiles. *J. Hydroinform.* **13** (3), 324–333.

Spalding, D. 1954 Mass transfer in laminar flow. *Proc. R. Soc. A* **221**, 78–99.

Sydberger, T. & Lotz, U. 1982 Relation between mass-transfer and corrosion in a turbulent pipe-flow. *J. Electrochem. Soc.* **129** (2), 276–283.

Tiselj, I., Horvat, A., Mavko, B., Pogrebnyak, E., Mosyak, A. & Hetsroni, G. 2004 Wall properties and heat transfer in near-wall turbulent flow. *Numer. Heat Tr. A-Appl.* **46** (7), 717–729.

Webb, R. L. & Kim, N. H. 2005 *Principles of Enhanced Heat Transfer*. Taylor & Francis.

Weigand, B. 2004 *Analytical Methods for Heat Transfer and Fluid Flow Problems*. Springer.

Weigand, B., Kanzamar, M. & Beer, H. 2001 The extended Graetz problem with piecewise constant wall heat flux for pipe and channel flows. *Int. J. Heat Mass Tran.* **44** (20), 3941–3952.

Zhao, W. & Trass, O. 1997 Electrochemical mass transfer measurements in rough surface pipe flow: geometrically similar V-shape grooves. *Int. J. Heat Mass Tran.* **40** (2), 2785–2797.